Spontaneous avalanche dephasing in large Rydberg ensembles

T. Boulier,[1,2] E. Magnan,[1,2] C. Bracamontes,[1] J. Maslek,[1] E. A. Goldschmidt,[3] J. T. Young,[1] A. V. Gorshkov,[1,4] S. L. Rolston,[1] and J. V. Porto[1,*]

[1]*Joint Quantum Institute, National Institute of Standards and Technology and the University of Maryland, College Park, Maryland 20742, USA*
[2]*Laboratoire Charles Fabry, Institut d'Optique Graduate School, CNRS, Université Paris-Saclay, 91127 Palaiseau cedex, France*
[3]*United States Army Research Laboratory, Adelphi, Maryland 20783, USA*
[4]*Joint Center for Quantum Information and Computer Science, National Institute of Standards and Technology and the University of Maryland, College Park, Maryland 20742, USA*

Strong dipole-exchange interactions due to spontaneously produced contaminant states can trigger rapid dephasing in many-body Rydberg ensembles [E. A. Goldschmidt *et al.*, Phys. Rev. Lett. **116**, 113001 (2016)]. Such broadening has serious implications for many proposals to coherently use Rydberg interactions, particularly Rydberg dressing proposals. The dephasing arises as a runaway process where the production of the first contaminant atoms facilitates the creation of more contaminant atoms. Here we study the time dependence of this process with stroboscopic approaches. Using a pump-probe technique, we create an excess "pump" Rydberg population and probe its effect with a different "probe" Rydberg transition. We observe a reduced resonant pumping rate and an enhancement of the excitation on both sides of the transition as atoms are added to the pump state. We also observe a time scale for population growth that is significantly shorter than predicted by homogeneous mean-field models, as expected from a clustered growth mechanism where high-order correlations dominate the dynamics. These results support earlier works and confirm that the time scale for the onset of dephasing is reduced by a factor which scales as the inverse of the atom number. In addition, we discuss several approaches to minimize these effects of spontaneous broadening, including stroboscopic techniques and operating at cryogenic temperatures. It is challenging to avoid the unwanted broadening effects, but under some conditions they can be mitigated.

I. INTRODUCTION

The dense level spacing of Rydberg atoms can be both a blessing and a curse. The strong polarizability of these highly excited states gives rise to giant interactions which, along with extended lifetimes, make them appealing candidates for engineering a variety of many-body Hamiltonians. Strong interactions are central to many-body experiments, including quantum magnetism [1,2] and quantum information processing [3–5]. Numerous proposals with varying levels of controllability and time scales use Rydberg interactions [1,6–14]. Importantly, Rydberg dressing proposals aim to engineer long-lived, interacting states by weakly admixing a Rydberg state with the ground state using off-resonant laser coupling [9–19]. While Rydberg dressing has been demonstrated for small atomic ensembles (100 atoms or fewer) and for short time scales [20,21], in the many-body regime success at coherent off-resonant dressing has been more elusive [22–26].

A major limitation not addressed by these proposals is a blackbody-induced avalanche dephasing effect, where the runaway production of atoms in strongly interacting contaminant states of opposite parity significantly decreases the available coherence time [20,22–24]. Given the potential applications of coherent Rydberg control, it is crucial to take such dissipative dynamics into account. Therefore, charting the properties of this source of decoherence is important for the development of Rydberg-based quantum computation and simulation. This work is such an effort, focusing on the dephasing's time dependence and impact on current research.

In order to study the time dependence of this broadening mechanism, we use a pump-probe technique where excitation to a "pump" Rydberg state induces broadening on a separate, "probe" Rydberg transition. Additionally, we study the early-time dynamics on a single Rydberg transition using both a stroboscopic approach and photon-counting measurements and show that homogeneous mean-field assumptions underestimate the speed of the avalanche process by an order of magnitude. This is a strong indication of the highly correlated, locally seeded nature of this avalanche process [27,28], which is relevant to the question of bistability in large, strongly interacting systems [29]. Both this correlated turn-on and the observation of a giant steady-state broadening rely on antiblockade mechanisms [29,30]. Finally, we discuss experimental parameters that might be tuned to extend coherence times, including operation at cryogenic temperatures and stroboscopic application of the excitation light.

II. EXPERIMENT

In a room-temperature radiation environment, a Rydberg atom has a significant probability to undergo a blackbody-stimulated transition to a Rydberg state of opposite parity [31,32], most probably changing the principal quantum number by 0 or 1. A single atom in such a state has extremely strong dipole exchange interactions with subsequently excited Rydberg atoms of the original parity [33–36]. For two atoms
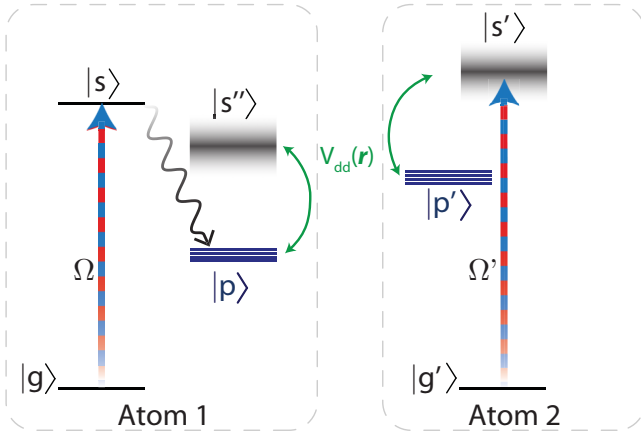
_____
*porto@umd.edu

FIG. 1. Interaction mechanism: Blackbody-dominated decay from the Rydberg state produces nearby *p* states ($|p\rangle$), which trigger an off-diagonal dipole-exchange interaction of the form $|p,s'\rangle \rightarrow |s'',p'\rangle$. This creates a dipole-dipole exchange interaction between two different Rydberg *s* states. For some orientation and distance **r** between the dipoles, this brings atom 2 into resonance and the excitation is enhanced (antiblockade). This energy shift inhomogeneously broadens the transition in the sample, as represented by the gray shading on $|s'\rangle$ and $|s''\rangle$. If $|s\rangle = |s'\rangle$, we are in the "self-broadening" situation where a single *s*-state transition is broadened via the *p* states created from it.

separated by $\boldsymbol{r}$, the interaction energy has the form [37,38]

$$\hat{V}_{dd}(\boldsymbol{r}) = \frac{1}{4\pi\epsilon_0} \frac{\hat{\boldsymbol{d}}_1 \cdot \hat{\boldsymbol{d}}_2 - 3(\hat{\boldsymbol{d}}_1 \cdot \boldsymbol{n})(\hat{\boldsymbol{d}}_2 \cdot \boldsymbol{n})}{|\boldsymbol{r}|^3}, \quad (1)$$

with $\boldsymbol{n} = \boldsymbol{r}/|\boldsymbol{r}|$, and where $\hat{\boldsymbol{d}}_i$ is the electric dipole operator of atom *i*. Because of the strength of the dipole interaction (scaling with the fourth power of the principal quantum number) and the $1/\boldsymbol{r}^3$ long-range character, a single perturber atom can affect many other atoms, potentially the entire sample. The contaminant atom shifts the transition energies of the atomic ensemble and modifies the remaining atoms' spectroscopic properties.

Figure 1 illustrates the generic case where *p* states originating from the decay of one *s*-state population dephase a different *s*-state transition ("cross broadening"). In the case where there is only one *s* state involved ($|s\rangle = |s'\rangle = |s''\rangle$ in Fig. 1), that state is dephased by the product of its own decay ("self-broadening").

We focus first on the simpler self-broadening mechanism: an off-resonant excitation (central to Rydberg dressing proposals) can resonantly excite atoms in the presence of contaminants, facilitating production of more contaminant Rydberg population [39] on both sides of the resonance. The process results in a rapid dephasing of the sample [40]. The interacting, dynamical excitation process can be complicated [28,29], but since it is triggered by the *first* blackbody decay, its onset occurs on a time scale that is *N* times faster than the single-atom scattering rate would indicate; here, *N* is the total number of atoms [20,24]. The subsequent runaway excitation quickly reaches steady-state Rydberg populations, effectively broadening the transition. Previous work explored the impact of similar, controlled

contaminant Rydberg populations [31,33–35]. However, the systematic appearance of uncontrolled contaminants has only recently been recognized [20,24] and a dynamic description was missing.

Since the resonant dipole interaction with the contaminant atoms exists for any of the various Zeeman or hyperfine states, cross broadening should occur between transitions to two different Rydberg states, as shown in Fig. 1. Contaminant population in state $|p\rangle$ produced by blackbody decay from $|s\rangle$ can broaden subsequent excitation to a separate state $|s'\rangle$. This suggests the possibility to study the broadening mechanism using a strong "pump" excitation to create contaminant Rydberg population, and a weak "probe" transition to measure the population's impact on linewidth. This approach has the benefit that the amount and time dependence of the contaminant population can be controlled independently from the probing transition [30]. Here we use excitation to two different Rydberg hyperfine states to study the broadening mechanism.

A. Experimental details

The details of our experimental setup are described in [24] and [41]. Briefly, the apparatus is used to create ^{87}Rb Bose-Einstein condensates (BECs) of $N \approx 4 \times 10^4$ atoms initially in the $|F = 1, m_F = -1\rangle$ ground state. Arbitrary fractions of the atoms can be transferred to any other state within the ground hyperfine manifold via microwave rapid adiabatic passage. We quantize the interatomic distances by loading the ^{87}Rb BECs into a three-dimensional (3D) optical lattice made with 812 nm light, resulting in a lattice spacing of 406 nm [41]. We then excite atoms to the $18S_{1/2}$ state using a two-photon transition via the $5P_{1/2}$ intermediate state [Fig. 2(a)]. The van der Waals (vdW) blockade radius is defined as the distance below which the interactions are larger than the collective two-photon Rabi frequency [42]: for the present experimental scheme, it is smaller than the lattice spacing. This corresponds to a vdW energy $E_{vdW} = 2\pi \times 2.1$ MHz. We note that the lattice is also instrumental in suppressing superradiant Rayleigh scattering [43]. The 485 nm light coupling $5P$ to $18S$ is common to both (pump and probe) two-photon transitions. The intermediate-state detuning is $|\Delta/2\pi| \approx 240$ MHz and the single-photon Rabi frequencies are independently calibrated: $\Omega_1/2\pi = 0$ to 10 MHz (on the $5S - 5P$ transition) and $\Omega_2/2\pi \approx 25$ MHz (on the $5P - 18S$ transition). The two lasers are stabilized to the same high-finesse optical cavity with <10 kHz linewidth, and are polarized and tuned to couple the ground hyperfine states to the desired $|18S_{1/2}, F_i, m_{F\,i}\rangle$ states (where $i = \{$probe, pump$\}$). Separate pump and probe excitation laser beams at the $5S - 5P$ transitions can be applied, while we apply only one $5P - 18S$ beam. The two-photon detunings δ_i and Rabi frequencies $\Omega_i = \Omega_{1,i}\Omega_{2,i}/2\Delta$ are independently tunable for each transition. The postexcitation populations in all of the ground hyperfine states (including those optically pumped to states different from $|g\rangle$ and $|g'\rangle$, the pump and probe states) are separated in time of flight with a Stern-Gerlach magnetic field gradient and measured via absorption imaging. We scan the various parameters and count the fractional population remaining in the ground states $|g\rangle$ and $|g'\rangle$ to obtain spectra of the transitions. The values and uncertainties of the widths
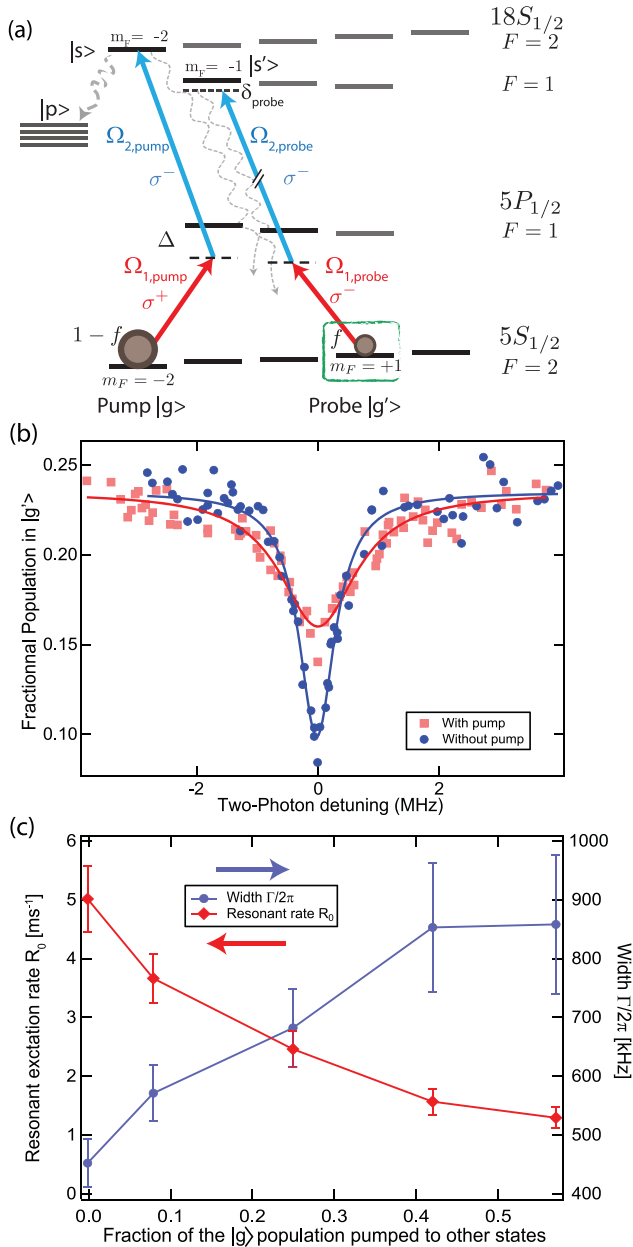
FIG. 2. Cross-state broadening. (a) The ground state is divided into a fraction f in the "probe state" $|g'\rangle$ (highlighted by a green square), leaving $1 - f$ in the "pump state" $|g\rangle$. Here $f = 0.25$, so that contaminant p atoms come predominantly from the pump while leaving enough atoms participating in the probe transition for a sufficient signal to noise ratio. The excitation to $18S$ is done via a two-photon transition with the $5P_{1/2}$ intermediate state: the intermediate detuning Δ is much greater than the single-photon Rabi frequencies and than the two-photon detuning δ_{probe} (not to scale on this figure). The pump population is driven resonantly to $|s\rangle = |18S,2,-2\rangle$ with two-photon Rabi frequency Ω_{pump}. (b) Example of broadening due to the presence of pump-induced Rydberg population. The blue (red) curve is the probe spectrum with the pump turned off (on). The fits are Lorentzian and are used to estimate the resonant rates R_0, the widths Γ, and their uncertainties throughout this work. (c) Probe transition widths and resonant excitation rates as a function of the fraction of $|g\rangle$ that was pumped to other states during the $300\,\mu$s excitation. We observe a doubling of Γ and a significant decrease of R_0 between no pump and the maximum pumped population.

presented in this work are derived from fits of these spectra, each containing at least 50 data points.

Figure 2(a) describes the pumping scheme: In the ground state, the atomic sample is divided into a small probe population (fractional density f) in a state $|g'\rangle = |5S,F = 2,m_F = 1\rangle$ within the ground manifold, and a large pump population (fractional density $1 - f$) in the state $|g\rangle = |5S,F = 2,m_F = -2\rangle$. The atoms are then excited to their respective pump or probe Rydberg state within the $18S$ hyperfine manifold via two-photon excitation: the pump is tuned to the $|g\rangle \rightarrow |s\rangle = |18S,F = 2,m_F = -2\rangle$ transition, while the probe is tuned near the $|g'\rangle \rightarrow |s'\rangle = |18S,F = 1,m_F\rangle$ transition, which is shifted by the $18S$ hyperfine splitting $\Delta_{\text{HF}} = 2\pi \times 10$ MHz. Here, $m_F = \{1,0,-1\}$ depends on the choice of probe laser polarization. We can pulse both 795 nm beams (probe and pump), which can be delayed by Δt relative to one another [see Fig. 3(a)]. The 485 nm light is kept on for the entire pulse sequence.

We also have access to the time-resolved total density of $18S$ atoms, through collection of the fluorescence photons emitted on the $5P_{3/2} - 5S_{1/2}$ transition [24]. The fluorescence scales with the optical pumping signal and is proportional to the number of $18S$ atoms. It is collected by a lens relay system (NA = 0.12) with an interference filter to block the $5S - 5P_{1/2}$ excitation light, detected by a single-photon avalanche diode, time tagged with 21 ns resolution, and summed over many repetitions. For technical reasons, including the fact that this method cannot discriminate between different states of the $18S$ hyperfine manifold, we use it to gain insight into the dynamics of the dephasing for a single transition (i.e., for the case of self-broadening).

B. Cross broadening

We first explore the cross broadening using the $|g'\rangle \rightarrow |s'\rangle = |18S,1,-1\rangle$ probe transition, shown in Fig. 2(a). With a fixed two-photon probe Rabi frequency $\Omega_{\text{probe}} = 2\pi \times 14$ kHz $\ll \Gamma_0$ and a single, simultaneous ($\Delta t = 0$) excitation time $t_p = 300\,\mu$s for both transitions, we take excitation spectra on the probe transition at different pump Rabi frequencies Ω_{pump}. $\Gamma_0/2\pi = 45$ kHz is the linewidth of the $18S$ transition, including blackbody radiation. Example spectra are shown in Fig. 2(b) for two cases: with and without pump excitation. The cross-broadened spectra are reasonably well described by Lorentzian functions, and we fit the data to extract the Lorentzian width Γ and the amplitude (along with their uncertainties). The average resonant excitation rate R_0 of probe atoms is determined from the fitted amplitudes, given the excitation time and the branching ratios to other states in the ground hyperfine manifold.

The probe spectra show a significant modification of both the resonant excitation rate and the width as a function of Ω_{pump}. We note that the range of available Ω_{pump} is limited by the constraint that the excitation time t_p must be long enough to give good signal to noise on the weakly excited probe transition. On the other hand, Ω_{pump} should not be so large as to significantly deplete the pump-state population in $|g\rangle$, in which case the steady-state population in Rydberg state $|s\rangle$ would decay during the probe pulse.
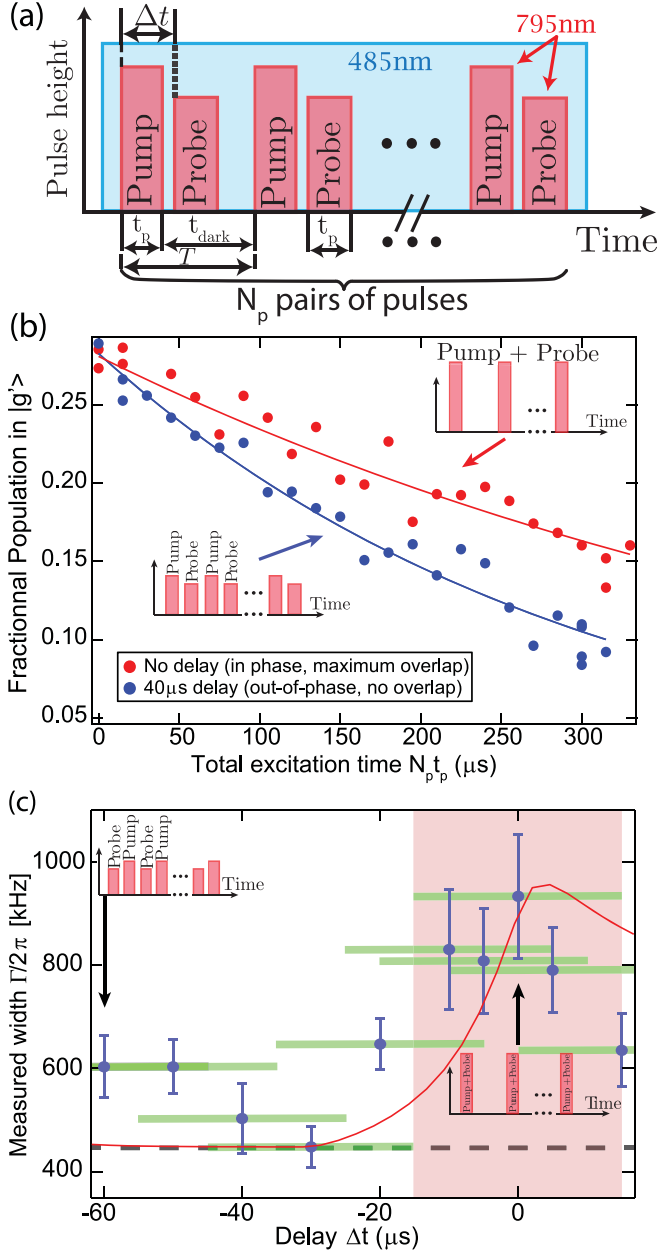
FIG. 3. Delayed pulses experiment. (a) To observe cross-broadening effects, we chop both 795 nm beams (probe and pump) into pulses, which can be delayed relative to one another. The 485 nm light is kept on. (b) Pump-induced slowdown of resonant excitation, visible in the number of atoms remaining in the probe ground state as a function of excitation time $N_p T$. The two examples here, fitted with exponentials, are for $\Delta t = 0 \, \mu$s (red) and $\Delta t = 40 \, \mu$s > t_p (blue). We observe rates of $R_{\Delta t = 0 \, \mu s} = 1.8 \pm 0.13$ ms^{-1} and $R_{\Delta t = 40 \, \mu s} = 3.3 \pm 0.14$ ms^{-1}. (c) Following the sequence in (a), we observe a broadening that depends on the overlap of the pulses. We focus on the turn on time (probe before pump, corresponding to negative δ for a pump pulse at $\Delta t = 0 \, \mu$s). The red zones represent the pump pulse, while the green bands show the probe pulse width. The gray dashed line is the (self-broadened) width obtained when the pump is turned off. Spectra corresponding to a high p population are obtained for $\Delta t \simeq 0 \, \mu$s and spectra corresponding to no pump population (pump turned off, marked by the dashed line) are recovered for $|\Delta t| \gtrsim t_p$. This is visible around $\Delta t = -40 \, \mu$s, when the probe is delayed well beyond the lifetime of the Rydberg states. The red line is the result of the nonlinear mean-field theory.

Figure 2(c) shows the probe width Γ and excitation rate R_0 for different $\Omega_{pump}/2\pi$ ranging from 0 to 20 kHz, plotted as a function of the fraction of atoms pumped out of the state $|g\rangle$ during the excitation time t_p. Note that this is proportional to the number of steady-state contaminant atoms, at least for small fractions. The width observed on the probe transition without pump is $\Gamma/2\pi \simeq 10\Gamma_0/2\pi = 450$ kHz, indicating some self-broadening. This is a constant effect for fixed Ω_{probe} and is compatible with the steady-state Ω scaling observed previously [24] on a single transition,

$$\Gamma \simeq \Omega\sqrt{\beta\rho_0}, \tag{2}$$

where ρ_0 is the density of ground-state atoms and β is an effective interaction volume inherent to the Rydberg state defined as

$$\beta = \sum \left|C_3^{(nP)}\right| b_{nP}\Gamma_{nP}^{-1}, \tag{3}$$

where the sum is over the nP states that have substantial dipole interactions with, and branching ratio from, the $18S$ state. Here, b_{nP} are the branching ratios to the nP states, Γ_{nP} are their decay rates, and $C_3^{(nP)}$ are effective dipole interaction strengths (including the root-mean-squared average of the angular dependence of C_3 [24]). When the pump is on, the width of the probe transition is increased by up to a factor of two, while the amplitude is reduced by four, showing that the pump creates a significant cross broadening due to the p-state population. The enhanced off-resonant excitation rate in the presence of the pump is indicative of pump-induced facilitation dynamics [30]. The observation of broadening between independent populations with independent transitions provides evidence for interaction between atoms and rules out superradiant broadening effects.

C. Cross-broadening dynamics

Atoms in s and p states can obviously only interact when present simultaneously. To demonstrate the simultaneous nature of the cross broadening, we chopped the 795 nm excitation light for both excitations into pulse trains and studied the effect of nonoverlapping pump and probe light. Each pulse had a length of $t_p = 30 \, \mu$s $\sim 10\tau_0$ separated by a dark time of $t_{dark} = 3t_p$, such that the total period was $T = 4t_p = 120 \, \mu$s. For fixed Rabi frequencies $\Omega_{probe} = 2\pi \times 15$ kHz and $\Omega_{pump} = 2\pi \times 20$ kHz (corresponding to the largest width seen in Fig. 2), we vary the delay Δt between the probe and the pump pulse trains. We chose t_p to be long compared to the onset of the avalanche dephasing, and the dark time following each pulse in both excitation (probe and pump) to be long with respect to the lifetime (3–10 μs) of the various s and p Rydberg populations.

As expected, the cross broadening and cross saturation are absent when the probe and pump pulses are out of phase. Figure 3(b) shows the resonant decay of $|g'\rangle$ at fixed $\delta_{probe} = \delta_{pump} = 0$ for two delays: $\Delta t = 0 \, \mu$s (overlap) and $\Delta t = 40 \, \mu$s (no overlap). The total excitation time is varied by changing the number of pulses, and the rates are extracted from exponential fits. The observed rate for simultaneous excitation ($R_{\Delta t = 0 \, \mu s} = 1.8 \pm 0.13$ ms^{-1}) is slower than for nonoverlapping excitation ($R_{\Delta t = 40 \, \mu s} = 3.3 \pm 0.14$ ms^{-1}). Figure 3(c) shows the extracted width for probe spectra taken

at different Δt. We observe a variation of the linewidth as a function of the delay. For $\Delta t = 0$ μs, we recover the same result as with the maximum p population in Fig. 2(c). We also observe the same width as without any pump light when the two pulse trains are nonoverlapping and separated by long enough dark times for their Rydberg populations to decay.

To study the dynamics of contaminant p-state population, we measured the probe spectral width as a function of pump-probe delay Δt over a full period T. For this experiment, we chose $|s'\rangle = |18S, F = 1, m_F = 1\rangle$ as a probe state. The $\Delta m_F = 3$ between the probe and the pump s states implies a process of the type $|p, s'\rangle \leftrightarrow |s'', p'\rangle$, where $|m_{F,p} - m_{F,s''}| \leqslant 1$ and $|m_{F,s'} - m_{F,p'}| \leqslant 1$, and where $|p\rangle \neq |p'\rangle$ and $|s'\rangle \neq |s''\rangle$ (since $|m_{F,p} - m_{F,s'}| \geqslant 2$). In order to get a significant two-photon Rabi frequency for both pump and probe transitions, we used as before an intermediate-state detuning $\Delta \approx 2\pi \times 240$ MHz, but this time blue detuned of the $|5S, F = 2\rangle \rightarrow |5P_{1/2}, F = 2\rangle$ transition [Fig. 4(a)]. Here, $t_p = 20$ μs and $T = 80$ μs. Figure 4(b) shows the width as a function of the delay. The largest value is observed for overlapping pulses, here too indicating that the pump pollutant population dephases the probe population. We note that the strength of the dipole exchange is almost the same as for the $|18S, F = 1, m_F = -1\rangle$ probe state, despite the fact that $\Delta m_F = 3$.

The shape and amplitude of the time-dependent signal are captured by a nonlinear rate-equation model, described below. It uses a single fit parameter, i.e., the effective interaction strength C_3^{cross} between the pump p state (s state) and the probe s state (p state). Interestingly, the model is consistently ~ 10 μs delayed with respect to the experiment; see the red solid lines in Figs. 3(c) and 4(b). As discussed below, this is likely a failure of the model's homogeneous mean-field assumptions to capture early-time dynamics due to strong local correlations (cluster dynamics) from which the pollutant population is seeded.

The cluster dynamics suggests a finite growth time. Therefore, for an excitation pulse short enough to avoid the p-state creation, the self-broadening might be avoided. Using a single $|5S \rightarrow 18S, F = 2, m_F = -2\rangle$ transition, we measured the linewidth as a function of pulse width t_p, using pulse trains in a similar fashion as shown in Fig. 3(a) but without probe light. Spectra were taken at different t_p while keeping the total excitation time $t_p N_p$ constant (where N_p is the number of pulses). To allow all excited population to decay in between pulses, the dark time was kept long compared to τ_0: $t_{\text{dark}} \simeq 20\tau_0 \simeq 10\Gamma_{\text{nP}}^{-1}$. The observed width is presented in Fig. 5. There is a clear decrease of the width at short times, up to three times narrower than the steady-state observations. At very short pulse widths, however, Fourier broadening begins to dominate, and the narrowing is limited to pulse times $t_p \gtrsim 2$ μs. We observe a time of about 10 μs to reach the steady state and infer a time scale of a few hundreds of nanoseconds for the onset of the broadening. The nonlinear rate-equation model (described below) captures the steady-state dephasing (outside the plot range) and the global shape of the time evolution. The speed at which the steady state is approached is, however, consistently underestimated by the model. As discussed below, this slow rise time is likely the result of the homogeneous mean-field assumption used here.
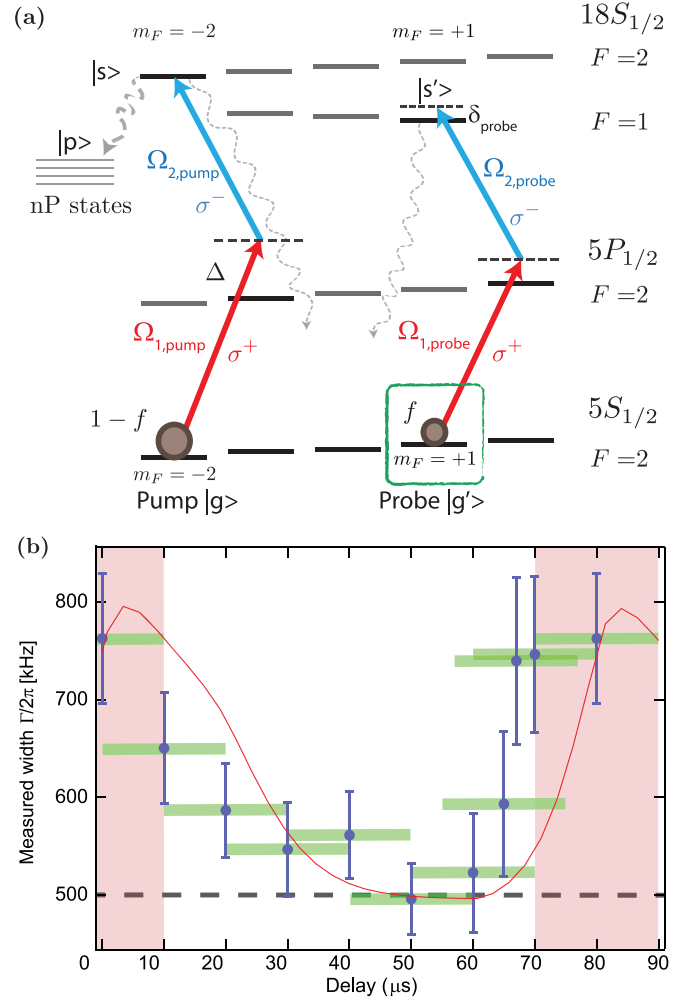

(a)

(b)

FIG. 4. The $\Delta m_F = 3$ case. (a) Pumping scheme for two states separated by $\Delta m_F = 3$. The pump population is driven resonantly to $|s\rangle = |18S, 2, -2\rangle$, while the probe transition is driven to $|s'\rangle = |18S, 1, +1\rangle$. (b) Time dependence of the pump-probe experiment. The red zones represent the times the pump is on, while the green bands show the probe pulse width. The gray dashed line is the (self-broadened) width obtained when the pump is turned off. Again we observe a spectral width increase when in phase, relative to out of phase. This plot spans the full period T and shows an asymmetry between having the probe after (0–40 μs) or before (40–80 μs) the pump. A rate-equation theory [see Eqs. (5)–(8)] shows (red line) the correct shape, including asymmetry, but consistently has a delay of ~ 10 μs.

D. Nonlinear rate-equation model

We compare the self-broadening data to a simple homogeneous nonlinear rate-equation model, which is a good approximation for situations with strong decoherence [27,44]. We approximate the system with three coupled populations [ground (g), Rydberg ($18S$), pollutant (nP)], treating all the pollutant states as a single effective state:

$$\dot{N}_g = (N_{18S} - N_g)R + \Gamma_0 b_1 N_{18S} + \Gamma_{\text{nP}} b_3 N_{\text{nP}}, \quad (4)$$

$$\dot{N}_{18S} = (N_g - N_{18S})R - \Gamma_0 N_{18S}, \quad (5)$$

$$\dot{N}_{\text{nP}} = b_2 \Gamma_0 N_{18S} - \Gamma_{\text{nP}} N_{\text{nP}}, \quad (6)$$
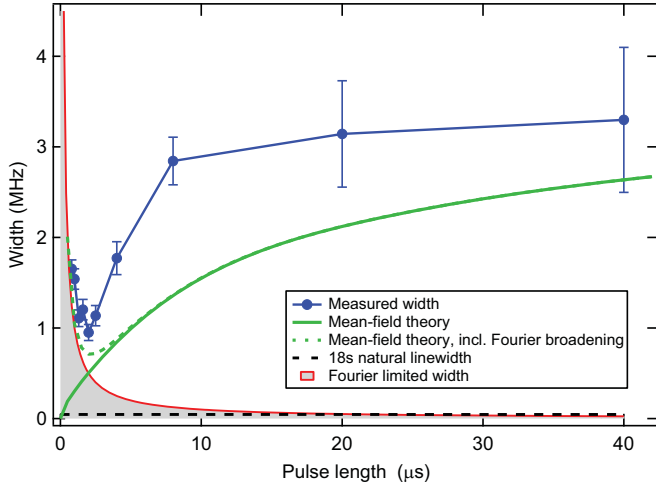
FIG. 5. Stroboscopic excitation on a single transition. Observed self-broadened width (blue) of the pump transition as a function of the individual pulse width. Here a single $|18S,2,-2\rangle$ population is excited with a Rabi frequency $\Omega = 2\pi \times 66$ kHz. Below $t_p \approx 3\tau_0$ (where τ_0 is the $18S$ lifetime), the broadening decreases, with a reduction of the width by a factor of ~ 3. However, the natural linewidth (black dashed line) cannot be recovered via this scheme due to the fundamental Fourier limit (red line, delimiting the forbidden region in gray). Here too the homogeneous mean-field prediction (green line) is slower than observed. The dashed green line shows the prediction for homogeneous mean-field plus Fourier broadening.

where $b_1 = 0.49$ is the branching ratio from the $18S$ states back to $|g\rangle = |5S, F = 2, m_F = -2\rangle$, $b_2 = \sum_{nP} b_2^{nP} = 0.18$ is the branching ratio of the decay from $|18S, F = 2, m_F = -2\rangle$ to the effective pollutant state, and $b_3 = 0.55$ is the branching ratio from the effective pollutant state back to $|g\rangle$. Decay of the total population represents atom loss and optical pumping to detection ground states. The interactions are modeled under a homogeneous mean-field assumption that the $18S$ dephasing rate depends on the typical density of pollutant atoms,

$$\Gamma(t) = \Gamma_0 + C_3 \rho_0 N_{nP}(t), \qquad (7)$$

where ρ_0 is the density of atoms (in any state), N_{nP} is the fraction of these atoms in the pollutant state, and $C_3 \simeq 2\pi \times 35$ MHz $\mu\mathrm{m}^3$ is the average of the $C_3^{(nP)}$ interaction strengths used in Eq. (2). The dephased excitation rate, including broadening and saturation, is then taken to be the time-dependent form

$$R(t) = \frac{\Gamma(t)}{2} \frac{2\Omega^2}{4\delta^2 + \Gamma^2(t)}. \qquad (8)$$

This model is consistent with the steady-state limit presented in Eq. (2). As shown in the Appendix, the model used for the cross-broadening experiment consists of a pair of such three-level systems coupled to each other by adding a cross-interaction term $C_3^{\mathrm{cross}} \rho_0 N_{nP}^{\mathrm{pump\,(probe)}}$ in the systems' respective dephasing rates $\Gamma^{\mathrm{probe\,(pump)}}$.

To compare with the experiment, we calculated (both for the self- and cross-broadening cases) the time dependence of the populations, starting with all atoms in the ground state(s). The optically pumped population that serves as our experimental signal is determined from the number of atoms remaining in the probe ground state at the end of the pulses, $N_g(t)$. This is repeated at a range of detunings to construct a simulated spectrum, from which we determine a width by fitting a Lorentzian.

For the delayed-pulse cross-broadening experiment, the model's results are shown as a red line in Figs. 3(c) and 4(b). It correctly predicts the overall time dependence with only one free parameter, C_3^{cross}, for which the extracted value is $C_3^{\mathrm{cross}} \simeq C_3/10 = 2\pi \times 3.5$ MHz $\mu\mathrm{m}^3$. It also captures the observed asymmetry on turn on and turn off of the pump in Fig. 4(b), but is delayed relative to the data by ~ 10 μs. We note that the time scale for relaxation to the probe-only width takes somewhat longer than the nP lifetime, which is indicative of the dynamics of facilitated excitation [29].

To gain better insight into this behavior, we look at the model's result for a pump-only pulsed excitation and compare it to the equivalent self-broadening experiment. This is shown as the green line in Fig. 5. Although the model tends to capture the late-times widths [24,28] (the experimental value is recovered at long times, outside of the plot range in Fig. 5), it consistently gives slower dynamics than observed experimentally. Since the growth of the pollutant population is expected to occur through an aggregation process similar to [39], strong correlations arise quickly after the first pollutant atom is created. A single atom in an nP state can shift some fraction of surrounding atoms into resonance, leading to fast excitation in an antiblockade, clustered dynamic [29,30]. Therefore, as recently highlighted [28], inhomogeneity and high-order correlations likely account for the faster experimental time scale.

This is confirmed by comparing the calculated $18S$ population dynamics to the corresponding experimental observation, obtained with fluorescence photon counting. The detected fluorescence (proportional to $18S$ population) vs time is presented in Fig. 6 for detunings $\delta/2\pi = 0, \pm 2.1$, and 3.9 MHz on a single transition (pump only). Here we chose $\Omega = 2\pi \times 140$ kHz. In all the data, the dephasing's effect appears earlier than in the homogeneous mean-field theory. For detuned light [Figs. 6(b) and 6(c)], the calculated facilitated excitation in the model happens on a time scale at least twice as long as in the experiment. For the resonant case [Fig. 6(a)], the decrease of the pumping rate (blockade effect) also happens later in the model, which manifests itself as a large overshoot at early times. This overshoot is also present in the data, but with a lower amplitude, indicating that the correlated dynamics starts the dephasing earlier. It is important to note that the presence of an overshoot in the data implies a finite time for the dephasing to occur. This demonstrates the existence of a third state (or set of states), since $18S - 18S$ interactions cannot produce such an overshoot. This state, the existence of which is directly demonstrated here, is necessarily the nP population, as verified by the experimental observations [20,22,24,45] in which it was originally inferred.

III. APPROACHES TO MITIGATE BROADENING

Given the range of applications of Rydberg atoms, it is worthwhile to consider possible approaches to minimize the impact of this decoherence mechanism.
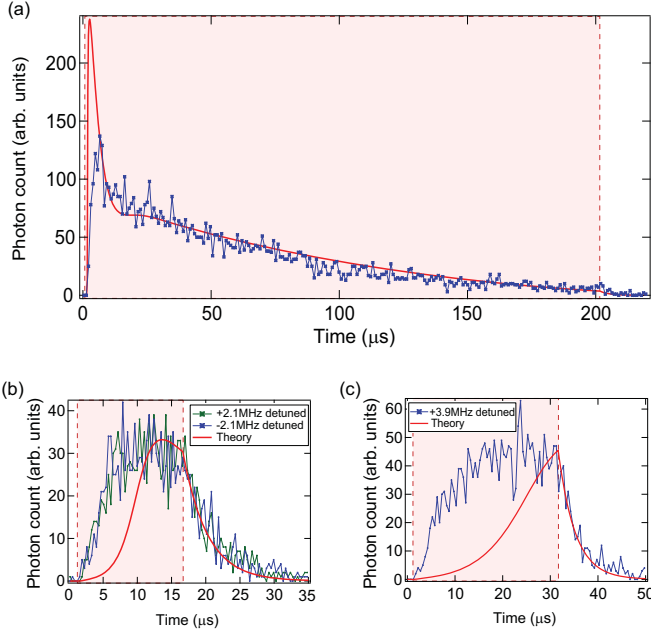
FIG. 6. Photon counting on a single transition. Observed $5P_{3/2} - 5S$ fluorescence (blue trace) vs time. The detected fluorescence is proportional to the $18S$ population. Here a single $|18S, 2, -2\rangle$ population is excited with a Rabi frequency $\Omega = 2\pi \times 140$ kHz (light red areas). The red line is the model. (a) Resonant case: an overshoot is visible in both the data and the model, signaling the presence of the nP population. Since the model is slower to produce pollutants, the overshoot in the model has more time to grow at the full single-particle rate than in reality. (b),(c) Detuned case: since the facilitated excitation relies on a pollutant population, the $18S$ population is slower to rise in the model than experimentally observed, confirming the faster-than-homogeneous mean-field property of the avalanche dephasing. Since the experimentally observed broadening is symmetric, the sign of the detuning does not change these observations.

A. Stroboscopic excitation

The fast but delayed turn on of the broadening shown in Figs. 5 and 6 indicates that the contaminant dephasing might be partially avoided by pulsing the Rydberg coupling on a short enough time scale t_p, followed by sufficiently long dark time t_{dark}. To allow for decay of any detrimental population, $t_{\text{dark}} = A\tau_0$, with $A \gg 1$ (to avoid the runaway process on the next pulse). The average time τ_c until the first contaminant-state atom appears provides an estimate of the actual coherent time available before the avalanche excitation is triggered. The associated rate τ_c^{-1} is roughly the number of atoms in the Rydberg state, $N(\frac{\Omega}{2\delta})^2$, times the rate at which this state decays to contaminant states. Therefore, given a sample with a total of N atoms participating in the dressed excitation, an estimate for τ_c is [24]

$$\frac{\tau_c}{\tau_0} = \frac{4\delta^2}{\Omega^2} \frac{1}{b_{\text{nL}} N} \equiv \frac{N_c}{N}, \tag{9}$$

where b_{nL} is the sum of the branching ratios from the general nL Rydberg-dressed state (with n the principal quantum number and $L = S, P, D, \ldots$ the angular momentum) to the

contaminant states contributing to the effective interaction volume β. $N_c = 4\delta^2/\Omega^2 b_{\text{nL}}$ is the number of atoms above which stroboscopic approaches will start to significantly diminish the dressing potential strength. The effective N may be suppressed (at short times) for systems in which a significant fraction of atoms is within a $|s\rangle - |s\rangle$ van der Waals blockade distance. However, the $|s\rangle - |p\rangle$ dipole-dipole interaction is much stronger and longer ranged than the van der Waals interaction, and once the contaminant $|p\rangle$ states are produced, the dipole broadening mechanism dominates. We note that since τ_0 increases with principle quantum number n (and b_{nL} increases weakly with n), increasing n will improve the overall time scale [42] before decoherence starts. Nevertheless, the decrease of τ_c with increasing atom number N is still present even at large n. Additionally, the situation is reversed after the first pollutant has appeared: C_3 increases with n and therefore, once started, the dephasing is stronger at higher n.

For experiments where the observable does not rely on correlations being preserved during the dark time and is on a much longer time scale than the total stroboscopic period T (which will not always be the case), the dressed interaction during $t_p < \tau_c$ could be averaged across many pulses. In principle, it would then be possible to avoid the avalanche dephasing. The available average interaction for a given coupling Ω and detuning δ would be decreased, however, by the duty cycle $t_p/T < \tau_c/(\tau_c + A\tau_0)$. The short-distance dressed interaction energy $U = \frac{\Omega^4}{8\delta^3}$ [17] is then limited to

$$U^* \lesssim \left(\frac{\Omega^4}{8\delta^3}\right) \frac{N_c/N}{A + N_c/N}. \tag{10}$$

For $N_c/N \gg A$, the stroboscopic approach gives a time-averaged interaction energy only slightly suppressed, $U^* \lesssim U$. In the opposite limit $N_c/N \ll A$ (which includes $N \gtrsim N_c$ since $A \gg 1$), the average interaction scales as $U^* \lesssim UN_c/AN \ll U$. For experimentally reasonable parameters of $\delta/\Omega \simeq 10$ and $b_{\text{nL}} \simeq 0.2$, $N_c \simeq 2000$. Fourier broadening provides a further fundamental limit to the stroboscopic approach. Avoiding Fourier-broadened excitation requires $\delta^{-1} \ll t_p < \tau_c$, which sets the additional constraint $N \ll N_c \delta/\Gamma_0$.

B. Cryogenic temperatures

The time τ_c before the first contaminant-state atom appears depends on the ambient temperature through b_{nL} and τ_0. This is shown in Figs. 7(a) and 7(b) for the example of ^{87}Rb nS Rydberg states. These plots were obtained using the estimates from Ref. [46] and the quasiclassical formulas in Ref. [47]. It is clear that lowering the ambient temperature increases τ_c, as well as increases the value of N_c for the stroboscopic approach. This is mainly due to the reduction of the branching ratio to nearby states b_{nL}. At room temperature, there is significant blackbody-driven decay to nearby states rather than by radiative decays to low-n states, due to the small energy difference between neighboring Rydberg states. Suppressing blackbody radiation at low temperatures makes the spontaneous decay to low-lying states the dominant channel.

Avalanche dephasing limits the coherence below the single-particle scattering time when $\tau_c < \frac{4\delta^2}{\Omega^2} \tau_0$. For a given
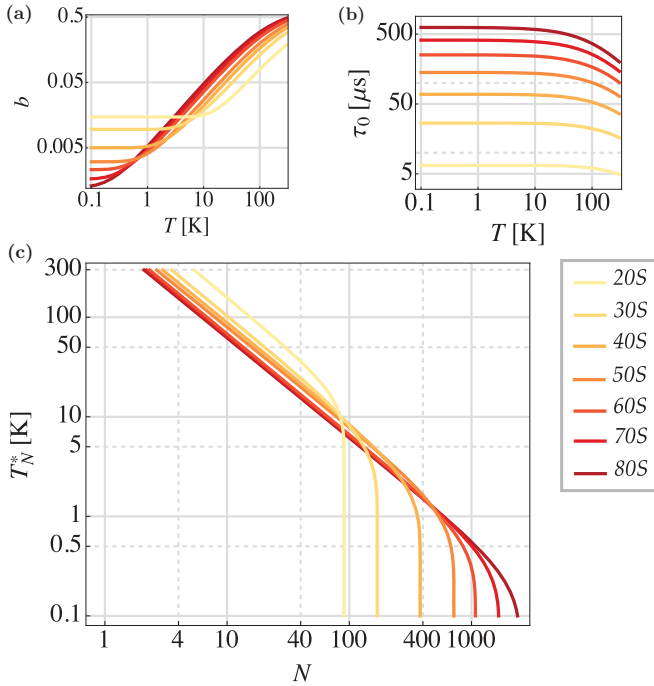
FIG. 7. Temperature scaling. (a) Temperature dependence of the sum of branching ratios b from the different nS states to the contaminant nP states playing a significant role in the avalanche dephasing process. (b) Effective lifetime τ_0 (determined by spontaneous emission and blackbody radiation-induced transitions) for different nS ^{87}Rb Rydberg states as a function of the ambient temperature. (c) Temperature T_N^* needed to compensate for the dephasing effect as a function of N. The sharp drop stems from the intrinsic branching ratio to contaminant states: even at zero temperature, there is a nonzero chance to produce a contaminant atom.

atom number N, we estimate the temperature T_N^* at which the dephasing time τ_c becomes smaller than the room-temperature single-particle scattering time, namely, the temperature at which $\tau_c(T_N^*) = \frac{4\delta^2}{\Omega^2}\tau_0(300\text{ K})$. T_N^* vs N is shown in Fig. 7(c).

Rydberg-dressing proposals [9–12] and experiments [20] making use of samples with $N \sim 30$–100 would need an ambient temperature near 10 K to make up for the avalanche dephasing effect. The detrimental effects of contaminant states on systems with even lower atom number ($N \sim 10$; see Refs. [13,14]), already small at room temperature, would become negligible for temperatures around liquid nitrogen, i.e., 77 K. On the other hand, avoiding contaminant dephasing in proposals relying on $N \gtrsim 10^3$, as in Ref. [24], does not seem feasible by going to lower temperatures. This is visible in Fig. 7(c) as a sharp drop to $T = 0$ K for the temperature needed to avoid the avalanche dephasing at high atom numbers, due to the always-finite value of spontaneous radiative decay rates.

A possible solution would be to suppress spontaneous decay with an off-resonant cavity in a sufficiently cold cryogenic environment (for example, dilution refrigerator techniques can reach $T \leqslant 0.1$ K), e.g., with a superconducting cavity.

For a conductor separation smaller than the spontaneous-emission wavelength, the Rydberg excitation cannot decay to vacuum modes and spontaneous decay is suppressed [48,49]. Suppressing both blackbody and spontaneous decay channels has the capacity to avoid the avalanche dephasing issue, despite substantial technical challenges.

C. Other approaches

Quenching contaminant atoms. One possibility to limit the impact of pollutants is to significantly shorten their lifetime so they do not live long enough to begin the avalanche process. This could be achieved, for example, by laser coupling the contaminant states to lower-lying, short-lived states. This approach should work in principle, but is challenging to realize experimentally because of the large number of states with appreciable C_3 coefficient with the targeted dressing state, requiring quenching of many states at once. Indeed, for a nS initial Rydberg state, there are at least four significant pollutant states: $nP_{1/2}$, $nP_{3/2}$, $(n-1)P_{1/2}$, and $(n-1)P_{3/2}$, plus all their hyperfine levels (if they are spectrally resolved). For an initial Rydberg state with $L \geqslant 1$, the number of significantly contributing neighbor states increases rapidly, requiring a large number of quenching lasers.

EIT dressing schemes. The idea of taking a new approach to Rydberg dressing [25] has also been discussed as a potential way out of the avalanche dephasing [42]. The idea presented in Ref. [25] uses resonant light in a two-atom electromagnetically induced transparency (EIT) condition to achieve a Rydberg dressinglike interaction potential. The double excitation to a Rydberg level of the atom pair can be tuned to a near-dark state (EIT condition). This reduces the Rydberg fraction of the final state, while achieving the same hallmarks as traditional Rydberg dressing. This method shows an increase of about an order of magnitude in the interaction strength compared to the usual dressing scheme for strontium, and is about as effective as the usual dressing for rubidium.

This scheme suffers as well from the avalanche dephasing: the dressing interaction stems from a nonzero Rydberg fraction, which can trigger the avalanche process in large ensembles. The data shows clear signs of early decoherence [23,25]. The tenfold improvement in U for strontium does, however, mean that fewer atoms are needed to achieve the same interaction energy as with the classic scheme. This presents an additional way to reduce somewhat the impact of the avalanche decoherence, at least for Rydberg systems with narrow intermediate-state transitions.

Postselection. Once triggered, the avalanche process occurs very quickly, resulting in dramatic ground-state excitation and loss. The authors in Ref. [20] took advantage of this fact by postselecting the experimental runs where the avalanche never occurred. While this approach does not effectively increase the average time scale for the experiment or change its scaling with N, it does allow for selecting contaminant-free data, at the expense of a decreased data rate. In Ref. [20], even for a relatively short experimental time $t \sim \tau_0(n)$ (the state lifetime) and for $N \simeq 100$, half the experimental runs were corrupted. We note that postselection could increase the parameter regime where stroboscopic approaches work, relaxing somewhat the constraints on that approach.

IV. CONCLUSION

In conclusion, we presented a set of experiments studying the rapid onset of decoherence systematically observed in large Rydberg ensembles. The data supports the proposed explanation [24] that the runaway production of atoms in contaminant Rydberg states, triggered by blackbody decay, is the source of the broadening. This decoherence mechanism is important to consider, as it should be present in any experiment with steady-state Rydberg population, such as Rydberg dressed systems or Rydberg-based quantum information processing. Our results also point towards the difficulty of avoiding the issue. We provide and discuss several ideas to reduce the impact of this effect, among which cryogenic operation has the highest figure of merit, especially if used in conjunction with cavity techniques, despite the inherent technical challenges. None of the proposed solutions, however, offer an easy way to evade the avalanche decoherence, but a combination of approaches may provide a way to mitigate the effect on current experiments.

On the other hand, this mechanism can be used to explore highly correlated, many-body dynamics [28], such as anti-blockade on both sides of the Rydberg transition ("anomalous facilitation" of excitation [30]), and related cluster growth dynamics [29,50]. The large (contaminant-induced) anomalous facilitation and the faster-than-homogeneous mean-field excitation rate seen here provide a strong indication of cluster growth dynamics in our system. In addition, such interaction-induced dephasing may have practical applications in few Rydberg systems, such as in the isolation of single-Rydberg excitations for entanglement generation [51].

ACKNOWLEDGMENTS

APPENDIX: CROSS-BROADENING RATE-EQUATION MODEL

As described in the main text, the simple three-level rate-equation model was extended to six states in order to account for the two (pump and probe) species and the cross interaction. This more general model takes into account both the effect of the pump on the probe and the effect of the probe on the pump. The full set of equations is

$$\dot{N}_{1,g}(t) = [N_{1,18S}(t) - N_{1,g}(t)]R_1(t) + b_{1,1}\Gamma_0 N_{1,18S}(t)$$
$$+ b_{3,1}\Gamma_{nP} N_{1,nP}(t) - \Gamma_{1,D} N_{1,g}(t), \quad \text{(A1)}$$

$$\dot{N}_{1,18S}(t) = [N_{1,g}(t) - N_{1,18S}(t)]R_1(t) - \Gamma_0 N_{1,18S}(t), \quad \text{(A2)}$$

$$\dot{N}_{1,nP}(t) = b_{2,1}\Gamma_0 N_{1,18S}(t) - \Gamma_{nP} N_{1,nP}(t), \quad \text{(A3)}$$

$$\dot{N}_{2,g}(t) = [N_{2,18S}(t) - N_{2,g}(t)]R_2(t) + b_{1,2}\Gamma_0 N_{2,18S}(t)$$
$$+ b_{3,2}\Gamma_{nP} N_{2,nP}(t) - \Gamma_{2,D} N_{2,g}(t), \quad \text{(A4)}$$

$$\dot{N}_{2,18S}(t) = [N_{2,g}(t) - N_{2,18S}(t)]R_2(t) - \Gamma_0 N_{2,18S}(t), \quad \text{(A5)}$$

$$\dot{N}_{2,nP}(t) = b_{2,2}\Gamma_0 N_{2,18S}(t) - \Gamma_{nP} N_{2,nP}(t), \quad \text{(A6)}$$

with the same mean-field assumption that the $18S$ dephasing rate depends on the typical density of pollutant atoms:

$$R_1(t) = \frac{\Gamma_1}{2} \frac{2\Omega^2}{\Gamma_1^2 + 4\delta_1^2}, \quad \text{(A7)}$$

$$R_2(t) = \frac{\Gamma_2}{2} \frac{2\Omega^2}{\Gamma_2^2 + 4\delta_2^2}, \quad \text{(A8)}$$

$$\Gamma_1 = \Gamma_0 + C_3\rho_0 N_{1,nP} + C_3^{Cross}\rho_0 N_{2,nP}, \quad \text{(A9)}$$

$$\Gamma_2 = \Gamma_0 + C_3\rho_0 N_{2,nP} + C_3^{Cross}\rho_0 N_{1,nP}, \quad \text{(A10)}$$

where $b_{1,i}$ is the branching ratio back to the ground state of species i, $b_{2,i} = \sum_{nP} b_{2,i}^{nP}$ is the branching ratio of the decay from the $18S$ state to the pollutant states, here taken as equal for $i = 1$ (pump) and $i = 2$ (probe), and $b_{3,i}$ is the branching ratio from the effective pollutant state of species i back to the ground state of the same species. δ_i is the two-photon detuning. Since the pump is always resonant in the experiment, we used $\delta_1 = 0$. The terms $-\Gamma_{i,D} N_{i,g}$ in the two ground-state equations correspond to the off-resonant scattering from the $5P_{1/2}$ state, with scattering rate $\Gamma_{i,D} = (\frac{\Omega_{1,i}}{2\Delta_i})^2 \Gamma_{5P}$ (with $\Gamma_{5P} = 2\pi \times 6$ MHz). Here we assume that the broadening energy scale is smaller than the hyperfine splitting and that the cross broadening and self-broadening can be treated independently. We set $C_3 \simeq 2\pi \times 34$ MHz μm^3, while C_3^{cross} is a fit parameter, found to be about $2\pi \times 3$ MHz. Γ_{nP}, C_3, and C_3^{cross} are taken to be the same for populations 1 and 2.

[1] D. Barredo, H. Labuhn, S. Ravets, T. Lahaye, A. Browaeys, and C. S. Adams, Coherent Excitation Transfer in a Spin Chain of Three Rydberg Atoms, Phys. Rev. Lett. **114**, 113002 (2015).

[2] H. Labuhn, D. Barredo, S. Ravets, S. de Léséleuc, T. Macrì, T. Lahaye, and A. Browaeys, Tunable two-dimensional arrays of single Rydberg atoms for realizing quantum Ising models, Nature (London) **534**, 667 (2016).

[3] H. Weimer, M. Müller, I. Lesanovsky, P. Zoller, and H. P. Büchler, A Rydberg quantum simulator, Nat. Phys. **6**, 382 (2010).

[4] T. Pohl, C. S. Adams, and H. R. Sadephpour, Cold Rydberg gases and ultra-cold plasmas, J. Phys. B **44**, 180201 (2011).

[5] M. Saffman, T. G. Walker, and K. Mølmer, Quantum information with Rydberg atoms, Rev. Mod. Phys. **82**, 2313 (2010).

[6] R. Heidemann, U. Raitzsch, V. Bendkowsky, B. Butscher, R. Löw, L. Santos, and T. Pfau, Evidence for Coherent Collective Rydberg Excitation in the Strong Blockade Regime, Phys. Rev. Lett. **99**, 163601 (2007).

[7] V. Bendkowsky, B. Butscher, J. Nipper, J. P. Shaffer, R. Löw, and T. Pfau, Observation of ultralong-range Rydberg molecules, Nature (London) **458**, 1005 (2009).

[8] E. Urban, T. A. Johnson, T. Henage, L. Isenhower, D. Yavuz, T. Walker, and M. Saffman, Observation of Rydberg blockade between two atoms, Nat. Phys. **5**, 110 (2009).

[9] G. Pupillo, A. Micheli, M. Boninsegni, I. Lesanovsky, and P. Zoller, Strongly Correlated Gases of Rydberg-Dressed Atoms: Quantum and Classical Dynamics, Phys. Rev. Lett. **104**, 223002 (2010).

[10] A. W. Glaetzle, R. Nath, B. Zhao, G. Pupillo, and P. Zoller, Driven-dissipative dynamics of a strongly interacting Rydberg gas, Phys. Rev. A **86**, 043403 (2012).

[11] I. Bouchoule and K. Mølmer, Spin squeezing of atoms by the dipole interaction in virtually excited Rydberg states, Phys. Rev. A **65**, 041803 (2002).

[12] A. W. Glaetzle, M. Dalmonte, R. Nath, I. Rousochatzakis, R. Moessner, and P. Zoller, Quantum Spin-Ice and Dimer Models with Rydberg Atoms, Phys. Rev. X **4**, 041037 (2014).

[13] R. M. W. van Bijnen and T. Pohl, Quantum Magnetism and Topological Ordering via Rydberg Dressing Near Förster Resonances, Phys. Rev. Lett. **114**, 243002 (2015).

[14] T. E. Lee, S. Gopalakrishnan, and M. D. Lukin, Unconventional Magnetism via Optical Pumping of Interacting Spin Systems, Phys. Rev. Lett. **110**, 257204 (2013).

[15] J. E. Johnson and S. L. Rolston, Interactions between Rydberg-dressed atoms, Phys. Rev. A **82**, 033412 (2010).

[16] N. Henkel, R. Nath, and T. Pohl, Three-Dimensional Roton Excitations and Supersolid Formation in Rydberg-Excited Bose-Einstein Condensates, Phys. Rev. Lett. **104**, 195302 (2010).

[17] J. Honer, H. Weimer, T. Pfau, and H. P. Büchler, Collective Many-Body Interaction in Rydberg Dressed Atoms, Phys. Rev. Lett. **105**, 160404 (2010).

[18] A. W. Glaetzle, M. Dalmonte, R. Nath, C. Gross, I. Bloch, and P. Zoller, Designing Frustrated Quantum Magnets with Laser-Dressed Rydberg Atoms, Phys. Rev. Lett. **114**, 173002 (2015).

[19] A. Dauphin, M. Müller, and M. A. Martin-Delgado, Rydberg-atom quantum simulation and chern-number characterization of a topological Mott insulator, Phys. Rev. A **86**, 053618 (2012).

[20] J. Zeiher, R. van Bijnen, P. Schauß, S. Hild, J.-y. Choi, T. Pohl, I. Bloch, and C. Gross, Many-body interferometry of a Rydberg-dressed spin lattice, Nat. Phys. **12**, 1095 (2016).

[21] Y.-Y. Jau, A. Hankin, T. Keating, I. Deutsch, and G. Biedermann, Entangling atomic spins with a Rydberg-dressed spin-flip blockade, Nat. Phys. **12**, 71 (2016).

[22] B. J. DeSalvo, J. A. Aman, C. Gaul, T. Pohl, S. Yoshida, J. Burgdörfer, K. R. A. Hazzard, F. B. Dunning, and T. C. Killian, Rydberg-blockade effects in Autler-Townes spectra of ultracold strontium, Phys. Rev. A **93**, 022709 (2016).

[23] J. A. Aman, B. J. DeSalvo, F. B. Dunning, T. C. Killian, S. Yoshida, and J. Burgdörfer, Trap losses induced by near-resonant Rydberg dressing of cold atomic gases, Phys. Rev. A **93**, 043425 (2016).

[24] E. A. Goldschmidt, T. Boulier, R. C. Brown, S. B. Koller, J. T. Young, A. V. Gorshkov, S. L. Rolston, and J. V. Porto, Anomalous Broadening in Driven Dissipative Rydberg Systems, Phys. Rev. Lett. **116**, 113001 (2016).

[25] C. Gaul, B. J. DeSalvo, J. A. Aman, F. B. Dunning, T. C. Killian, and T. Pohl, Resonant Rydberg Dressing of Alkaline-Earth Atoms via Electromagnetically Induced Transparency, Phys. Rev. Lett. **116**, 243001 (2016).

[26] J. B. Balewski, A. T. Krupp, A. Gaj, S. Hofferberth, R. Löw, and T. Pfau, Rydberg dressing: understanding of collective many-body effects and implications for experiments, New J. Phys. **16**, 063012 (2014).

[27] C. Ates, T. Pohl, T. Pattard, and J. M. Rost, Many-body theory of excitation dynamics in an ultracold Rydberg gas, Phys. Rev. A **76**, 013413 (2007).

[28] J. T. Young, T. Boulier, E. Magnan, E. A. Goldschmidt, R. M. Wilson, S. L. Rolston, J. V. Porto, and A. V. Gorshkov, Dissipation induced dipole-dipole blockade in driven-dissipative Rydberg systems, arXiv:1710.01752

[29] F. Letscher, O. Thomas, T. Niederprüm, M. Fleischhauer, and H. Ott, Bistability Versus Metastability in Driven Dissipative Rydberg Gases, Phys. Rev. X **7**, 021020 (2017).

[30] F. Letscher, O. Thomas, T. Niederprüm, H. Ott, and M. Fleischhauer, Anomalous excitation facilitation in inhomogeneously broadened Rydberg gases, Phys. Rev. A **95**, 023410 (2017).

[31] W. R. Anderson, J. R. Veale, and T. F. Gallagher, Resonant Dipole-Dipole Energy Transfer in a Nearly Frozen Rydberg Gas, Phys. Rev. Lett. **80**, 249 (1998).

[32] W. E. Cooke and T. F. Gallagher, Effects of blackbody radiation on highly excited atoms, Phys. Rev. A **21**, 588 (1980).

[33] H. Park, P. J. Tanner, B. J. Claessens, E. S. Shuman, and T. F. Gallagher, Dipole-dipole broadening of Rb nsnp microwave transitions, Phys. Rev. A **84**, 022704 (2011).

[34] G. Günter, H. Schempp, M. Robert-de Saint-Vincent, V. Gavryusev, S. Helmrich, C. S. Hofmann, S. Whitlock, and M. Weidemüller, Observing the dynamics of dipole-mediated energy transport by interaction-enhanced imaging, Science **342**, 954 (2013).

[35] E. Brekke, J. O. Day, and T. G. Walker, Excitation suppression due to interactions between microwave-dressed Rydberg atoms, Phys. Rev. A **86**, 033406 (2012).

[36] H. Park, T. F. Gallagher, and P. Pillet, Microwave pump-probe spectroscopy of the dipole-dipole interaction in a cold Rydberg gas, Phys. Rev. A **93**, 052501 (2016).

[37] K. Afrousheh, P. Bohlouli-Zanjani, D. Vagale, A. Mugford, M. Fedorov, and J. D. D. Martin, Spectroscopic Observation of Resonant Electric Dipole-Dipole Interactions Between Cold Rydberg Atoms, Phys. Rev. Lett. **93**, 233001 (2004).

[38] A. Browaeys, D. Barredo, and T. Lahaye, Experimental investigations of dipole–dipole interactions between a few Rydberg atoms, J. Phys. B **49**, 152001 (2016).

[39] A. Urvoy, F. Ripka, I. Lesanovsky, D. Booth, J. P. Shaffer, T. Pfau, and R. Löw, Strongly Correlated Growth of Rydberg Aggregates in a Vapor Cell, Phys. Rev. Lett. **114**, 203002 (2015).

[40] U. Raitzsch, R. Heidemann, H. Weimer, B. Butscher, P. Kollmann, R. Löw, H. Büchler, and T. Pfau, Investigation of dephasing rates in an interacting Rydberg gas, New J. Phys. **11**, 055014 (2009).

[41] Y.-J. Lin, A. R. Perry, R. L. Compton, I. B. Spielman, and J. V. Porto, Rapid production of r 87 b Bose-Einstein condensates in a combined magnetic and optical potential, Phys. Rev. A **79**, 063631 (2009).

[42] M. Saffman, Quantum computing with atomic qubits and Rydberg interactions: Progress and challenges, J. Phys. B **49**, 202001 (2016).

[43] S. Inouye, A. Chikkatur, D. Stamper-Kurn, J. Stener, D. Pritchard, and W. Ketterle, Superradiant Rayleigh Scattering from a Bose-Einstein Condensate, Science **285**, 571 (1999).

[44] M. Höning, D. Muth, D. Petrosyan, and M. Fleischhauer, Steady-state crystallization of rydberg excitations in an optically driven lattice gas, Phys. Rev. A **87**, 023401 (2013).

[45] T. F. Gallagher, *Rydberg Atoms* (Cambridge University Press, Cambridge, 2005), Vol. 3.

[46] I. I. Beterov, I. I. Ryabtsev, D. B. Tretyakov, and V. M. Entin, Quasiclassical calculations of blackbody-radiation-induced depopulation rates and effective lifetimes of Rydberg ns, np, and nd alkali-metal atoms with $n \leqslant 80$, Phys. Rev. A **79**, 052504 (2009).

[47] L. G. D'yachkov and P. M. Pankratov, On the use of the semiclassical approximation for the calculation of oscillator strengths and photoionization cross sections, J. Phys. B **27**, 461 (1994).

[48] D. Kleppner, Inhibited Spontaneous Emission, Phys. Rev. Lett. **47**, 233 (1981).

[49] R. G. Hulet, E. S. Hilfer, and D. Kleppner, Inhibited Spontaneous Emission by a Rydberg Atom, Phys. Rev. Lett. **55**, 2137 (1985).

[50] D. Petrosyan, M. Höning, and M. Fleischhauer, Spatial correlations of Rydberg excitations in optically driven atomic ensembles, Phys. Rev. A **87**, 053414 (2013).

[51] F. Bariani, Y. Dudin, T. Kennedy, and A. Kuzmich, Dephasing of Multiparticle Rydberg Excitations for Fast Entanglement Generation, Phys. Rev. Lett. **108**, 030501 (2012).